

## Postcollision interaction effects induced by Auger cascades following Xe $L_3$ -shell ionization

T. Hayaishi,<sup>1</sup> E. Murakami,<sup>2</sup> Y. Lu,<sup>3</sup> E. Shigemasa,<sup>4</sup> A. Yagishita,<sup>4</sup> F. Koike,<sup>5</sup> and Y. Morioka<sup>3</sup>

<sup>1</sup>*Institute of Applied Physics, University of Tsukuba, Tsukuba, Ibaraki 305, Japan*

<sup>2</sup>*Department of Physics, Chiba Institute of Technology, Narashino, Chiba 275, Japan*

<sup>3</sup>*Institute of Physics, University of Tsukuba, Tsukuba, Ibaraki 305, Japan*

<sup>4</sup>*Photon Factory, National Laboratory for High Energy Physics, Tsukuba 305, Japan*

<sup>5</sup>*School of Medicine, Kitasato University, Sagamihara, Kanagawa 228, Japan*

(Received 5 April 1996)

Yield spectra of multiply charged ions have been measured in coincidence with threshold electrons near the Xe  $L_3$ -shell ionization region. The ion-yield spectra exhibit characteristic profiles of postcollision interaction effects induced by Auger cascades following Xe  $L_3$ -shell ionization. The peak shifts of the spectral profiles increase gradually along with the increase of the charge states, but the peak widths are almost independent of the charge states. The spectral profiles are reproduced by a simple model based on the assumption that Coster-Kronig and Auger shake-off decays play a major role in the Auger cascades following the Xe  $L_3$ -shell vacancy creation. [S1050-2947(96)01111-0]

PACS number(s): 32.80.Hd, 32.70.-n

### I. INTRODUCTION

Postcollision interaction (PCI) effects often occur in Auger decays following near-threshold inner-shell photoionization of atoms. The PCI effect is caused by a sudden change of the Coulomb field that a faster Auger electron experiences on overtaking an initially ejected slower photoelectron. The faster Auger electron gains energy in the sudden change and, as its counterpart, the slower photoelectron loses energy by the same amount. As a result, the energy distributions of the photoelectrons and Auger electrons obtain characteristic line shapes; the shapes are asymmetric and broadened, and their maximum is shifted in energy.

Most of the previous studies on the PCI effects have concerned a single step of the Auger decay both in experiment and in theory (for example, see Schmidt [1]). Recently, Hayaishi *et al.* [2] observed the PCI profiles induced by Auger cascades following Ar  $K$ -shell photoionization, using a threshold electron-photoion coincidence technique. The Auger cascade causes the peak shift of the PCI profiles to increase gradually along with the increase in the number of Auger decays, but the peak width is almost constant. This experimental finding cannot be explained by any conventional PCI theories (for example, Russek and Mehlhorn [3], Armen *et al.* [4], Read and Hammond [5], and van der Straten *et al.* [6]); in these theories, in contrast to the present experimental results, the peak width increases as the peak shift increases. The observed PCI profiles were analyzed in terms of a simple model expressing the probability of Auger electron emission by statistical weights [2]. Koike [7] has proposed a formula to represent the PCI profiles, taking into account the time ordering of the cascading transitions. Although they are the ones at higher excess energies, Sheinerman [8] has calculated the PCI distorted profiles of a photoelectron in the formation of triply charged ions, taking into account the Coulomb final-state interaction in the Auger cascade.

The aim of the present study is to examine the PCI profiles produced by Auger cascades after Xe  $L_3$ -shell photoion-

ization, in which the number of the cascading steps is larger than that in the case of Ar  $K$ -shell photoionization. The profiles are measured by the threshold electron-photoion coincidence technique. The Xe  $L_3$ -shell ionization process induces sequential vacancy transfer, such as radiative, Auger, and Coster-Kronig decays [9], and the decay results in the production of multiply charged ions according to each decay channel [10,11]. Measurements of multiply charged ions in coincidence with threshold electrons thereby allow us to observe the PCI effects, depending on the decay channels of the Auger cascades following the Xe  $L_3$ -shell ionization. The previous study of argon deals with five stages of Auger cascades, whereas this study of xenon involves eight stages of Auger cascades plus many more Coster-Kronig-type transitions. Here, the term Auger cascades will be used throughout this paper to include Coster-Kronig decays as well as Auger decays.

### II. EXPERIMENT

Experiments were carried out at the undulator beam line BL-2A in the 2.5-GeV-electron storage ring of the Photon Factory at the National Laboratory for High Energy Physics [12]. The beam line is equipped with a silicon double-crystal monochromator [13]. The bandwidth of the monochromator was about 1 eV at 5000-eV photon energy. Multiply charged ions were measured in coincidence with threshold electrons using a time-of-flight mass spectrometer coupled with a threshold-electron-energy analyzer [14]. The energy resolution of the threshold-electron analyzer was estimated to be about 0.03 eV. The photon energy scale was calibrated by setting the peak maximum of the total-yield spectrum to 4787.3 eV [15,16].

### III. RESULTS AND DISCUSSION

Figure 1 shows yield spectra of total ions, threshold electrons, and multiply charged ions near the Xe  $L_3$ -shell ionization threshold in the threshold-electron-photoion coincidence measurement. These yield spectra were normalized

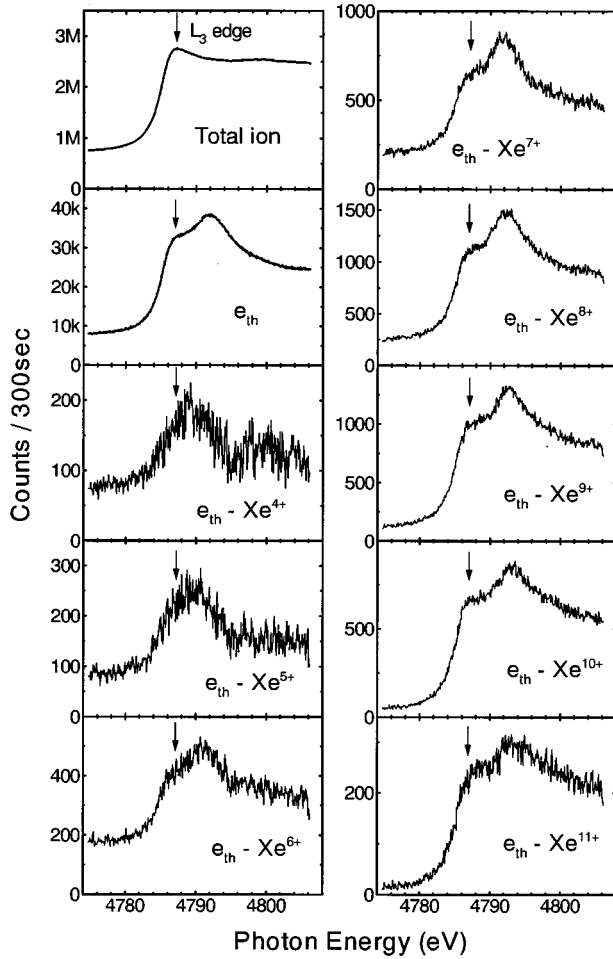


FIG. 1. Yield spectra of total ions, threshold electrons, and multiply charged ions in coincidence with threshold electrons near the Xe  $L_3$ -shell photoionization region. The notation  $e_{th}$  denotes the threshold electrons. Arrows indicate the Xe  $L_3$ -shell ionization edge [15,16].

with respect to the intensity of the radiation from the monochromator. The yield spectrum of the total ions, taken without mass analysis, corresponds to a photoabsorption spectrum [16,17]. The spectrum exhibits clearly the Xe  $L_3$ -shell ionization edge. The yield spectrum of the threshold electrons also exhibits the  $L_3$ -shell ionization edge and, in addition, the PCI distorted  $L_3$  photoline above the ionization edge. This threshold-electron emission induces the production of multiply charged ions from  $Xe^{4+}$  to  $Xe^{11+}$ ; that is, these yield spectra of the multiply charged ions reveal components of the decay channels accompanying threshold-electron emission. Figure 2 shows the main decay channels of the Xe  $L_3$ -shell hole state. The productions of the multiply charged ions are due to not only Auger decays but also to Coster-Kronig and Auger shake-off (double Auger) decays [9,18,19]. The  $L_3$ - $M_{45}M_{45}$  and  $L_3$ - $M_3M_{45}$  transitions are dominant decays [9]. This is in agreement with the experimental fact that  $Xe^{8+}$  and  $Xe^{9+}$  ions are the main products.

The threshold-electron spectra, which illustrate the PCI spectral shapes associated with various charge states of Xe ions, are the superposition of the PCI spectral profile due to

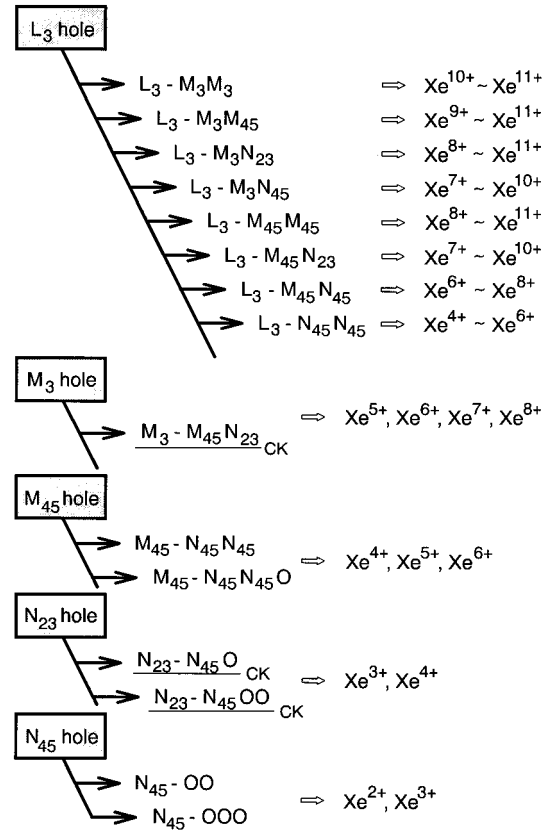


FIG. 2. Charge states resulting from the opening of a given subshell in xenon. Decays from the  $L_3$ -shell hole state constitute main channels [9]. Sequential decays from the  $M$ - and  $N$ -shell double-hole states result in the production of multiply charged ions [18,19]. The expected charge states are shown on the right-hand side. The notation CK signifies Coster-Kronig transitions.

the  $L_3$ -shell ionization and additional contributions to the coincident threshold-electron spectrum. The additional contributions arise from double Auger decays (shake off accompanying normal Auger decays), shake-off in the direct photoionization of higher-lying subshells, and secondary Auger decay processes that lead to the emission of very slow electrons. To pick out the PCI shapes from the threshold-electron spectra, we subtract all contributions other than the PCI line shape, assuming that they are similar in form to the total-ion-yield spectrum, and also subtract the background, assuming that it is almost photon-impact-energy independent in the energy range of concern. Those assumptions may be justified if one keeps in mind that we can anticipate the emission of at least one electron with near-zero kinetic energy from the multielectron emission process. Figure 3 shows the result of the subtraction. The spectra of the multiply charged ions exhibit distinct PCI profiles. The spectral profiles are asymmetric and broadened, and those maxima are shifted in energy from the Xe  $L_3$ -shell ionization edge.

Table I lists the peak shifts and widths estimated from those yield spectra of Fig. 3, including convolution with the monochromator bandpass using triangle profiles [20,21]. The PCI profile in the  $L_3$ - $M_4M_5$  ( $^1G_4$ ) Auger electron spectrum of xenon has been measured by Brown *et al.* [22] and Armen

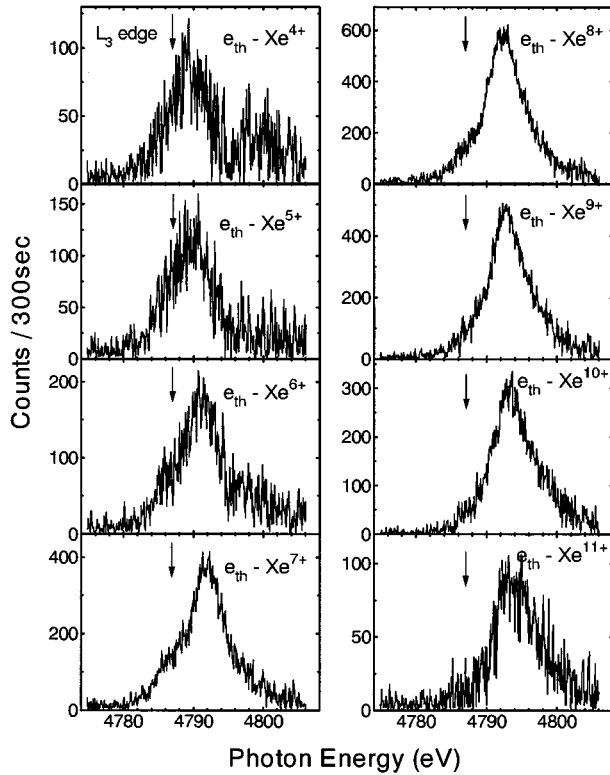


FIG. 3. Yield spectra of the multiply charged ions in coincidence with threshold electrons near the Xe  $L_3$ -shell photoionization region. These yield spectra were obtained by elimination of all processes not associated with the PCI profiles and the background due to outer-shell ionization from the yield spectra of Fig. 1. The notation  $e_{th}$  denotes the threshold electrons. Arrows indicate the Xe  $L_3$ -shell ionization edge [15,16].

*et al.* [23]. The  $L_3$ - $M_4M_5$  Auger decay mainly results in the production of  $Xe^{8+}$  and  $Xe^{9+}$  ions, as seen in Fig. 2. The present peak widths for these charged ions are in agreement with the 6.1-eV value estimated by them, although both were

TABLE I. Peak shifts (eV) and widths (eV) of the PCI profiles appearing in the yield spectra of multiply charged ions in Fig. 3. These values were determined after convoluting the PCI profiles with a triangle profile to account for the bandpass of the incident x rays. The peak shifts are estimated from the Xe  $L_3$ -shell ionization edge and the peak widths are estimated from the full widths at half maximum of each peak. For comparison, those amounts obtained by theoretical calculations are included (see text).

Charge state	Experiment		Calculation		Profile
	Shift	Width	Shift	Width	
$Xe^{4+}$	2.0 ( $\pm 1$ )	5.5 ( $\pm 1$ )	3.0	4.8	$^2P$
$Xe^{5+}$	3.0 ( $\pm 1$ )	5.6 ( $\pm 1$ )	3.7	5.4	$^2P+^3P$
$Xe^{6+}$	4.0 ( $\pm 1$ )	5.9 ( $\pm 1$ )	4.2	5.4	$^3P$
$Xe^{7+}$	4.5 ( $\pm 1$ )	5.9 ( $\pm 1$ )	4.6	5.8	$^3P+^4P$
$Xe^{8+}$	4.9 ( $\pm 1$ )	6.1 ( $\pm 0.5$ )	4.9	5.8	$^4P$
$Xe^{9+}$	5.3 ( $\pm 1$ )	6.0 ( $\pm 0.5$ )	5.4	6.0	$^4P+^5P$
$Xe^{10+}$	5.8 ( $\pm 1$ )	6.5 ( $\pm 0.5$ )	5.6	6.1	$^5P$
$Xe^{11+}$	6.2 ( $\pm 1$ )	6.6 ( $\pm 0.5$ )	6.0	6.1	$^5P+^6P$

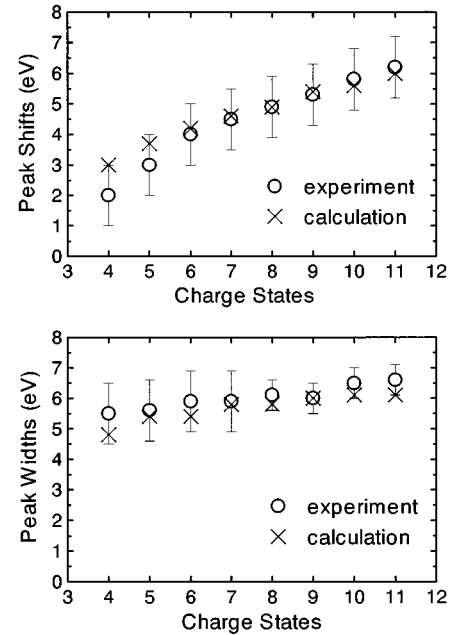


FIG. 4. Peak shifts and widths induced by the PCI effects as a function of charge states. Open circles indicate those amounts estimated from the PCI profiles of Fig. 3. Crosses indicate those obtained in theoretical calculations (see text).

measured with low resolution. On the other hand, the present peak shifts for these charge states are in disagreement with the 3.5-eV value estimated by them. This difference for the peak shifts is ascribable to multistep decays in the Auger cascades from the Xe  $L_3$ -shell vacancy, as mentioned below. Figure 4 shows the peak shifts and widths of the PCI profiles as a function of charge states. Notice that the peak shift increases gradually according to the increase of the charge states, but the peak width is almost insensitive to the increase. This remarkable tendency is the same as that found in the PCI profiles created by the Ar  $K$ -shell photoionization [2].

On the basis of a simple model expressing the probability of Auger-electron emissions by statistical weights [2], the PCI profiles of argon were represented by the following formula:

$${}^n P_A(\varepsilon_S) = \frac{g_n^n}{(n-1)!} \frac{\exp(-g_n/\varepsilon_S)}{\varepsilon_S^{(n+1)}}, \quad (1)$$

$$g_n = n[\ln(n + \frac{1}{2}) + \gamma],$$

where  $n$  is the number of Auger steps in the Auger cascades; that is,  $n+1$  corresponds to the charge number of the ionic state,  $\gamma=0.5772\dots$  is Euler's constant, and  $\varepsilon_S$  is the scaled energy  $\varepsilon_S=(v/\Gamma)E$ . This relation is expressed in atomic units. The scaled energy is expressed by the energy gain  $E$  measured from the nominal position of the photoelectron or Auger-electron peak, the lifetime width  $\Gamma$  of the core-hole state, and the photoelectron velocity  $v$ .

This  ${}^n P$  profile formula needs to be modified to some extent to be applied to the case of xenon. In the application of the original  ${}^n P$  formula to the experimental PCI profiles, any reasonable fit for the adjustable parameter  $\Gamma/v$  between

theoretical and experimental profiles cannot be obtained. This problem is due to participation of more complicated decays in the Xe  $L_3$ -shell ionization than those in the Ar  $K$ -shell ionization. It should be noted that Coster-Kronig decays play a major role in the Auger cascades following the Xe  $L_3$ -shell ionization, as seen in Fig. 2. The Coster-Kronig decay is dominant in the decay of the  $M_3$ -shell vacancy following the decay of the  $L_3$ -shell vacancy of xenon, such as the  $M_3$ - $M_{45}N_{23}$  Coster-Kronig decay [9,18]. Furthermore, in the  $N_{23}$ -shell vacancy of xenon, the Coster-Kronig decay also is dominant in the vacancy transfer, such as  $N_{23}$ - $N_{45}O_{23}$ . In general, the Coster-Kronig decay is much faster than the usual Auger decay. According to Keski-Rahkonen and Krause [24], the Coster-Kronig width  $\Gamma_C$  from the  $M_{23}$  shell is about 5 eV, whereas the relevant Auger width  $\Gamma_A$  is about 0.6 eV, which are quite different from each other. Our previous assumption does not hold if both Auger and Coster-Kronig decays are present in a cascade, because the profile formula in Eq. (1) assumes that the decay rate is the same in every cascading step. The faster decay of the Coster-Kronig transition causes a larger PCI effect in comparison with the relevant Auger decay. The PCI effect due to the Auger decays therefore is hidden by the large effects due to the Coster-Kronig decays. As a result, the PCI effect is enhanced at every decay step due to the Coster-Kronig transition, but the effective number of steps in the cascade is reduced.

The reduction of  $n$  in the cascades may also be caused by Auger shake-off decays in addition to the Coster-Kronig decays. One or more electrons could be shaken off, accompanying the emission of an Auger electron during the Auger decay. This Auger shake-off decay leads to a reduction of the effective number of steps in the cascade. According to the measurement of multiply charged ions by Saito and Suzuki [18], the probability of the Auger shake-off decays is 40% in decays from Xe  $M$ -shell ionization.

Table I lists peak shifts and widths of the PCI profiles calculated on the assumption that the  $^n P$  formula is applied to the profile of the  $2n$  charge state. The peak shifts and widths, displayed by crosses in Fig. 4, were estimated from the  $^n P$  formula using a value for the adjustable parameter  $\Gamma/\nu=3$ . Figure 4 exhibits a consistency with the theory and experiment in this choice for the adjustable parameter. These peak shifts and widths for the charge states beyond the  $\text{Xe}^{6+}$  ions are in good agreement with the experimental results, although the assumption for the effective number of steps is not explicit. The disagreement for  $\text{Xe}^{4+}$  and  $\text{Xe}^{5+}$  ions is considered as follows. Auger decays are more dominant than Coster-Kronig decays in the decays ending up with the production of these charge states. The value of the adjustable parameter  $\Gamma/\nu=3$  is unsuitable in the application of Eq. (1) to these charge states.

Although a small discrepancy exists between the theory and experiment, as pointed out above, we may conclude as follows: regarding the overall behavior of the PCI profiles, the PCI profiles induced by the Auger cascades following the Xe  $L_3$ -shell photoionization were overall successfully reproduced by Eq. (1), in consideration of the Auger cascades accompanied by the Coster-Kronig and Auger shake-off decays. However, it will be necessary for us to discuss the PCI effects of Auger cascades by using a more precise treatment.

#### ACKNOWLEDGMENTS

We are grateful to Professor J. A. R. Samson for a critical reading of this manuscript. We are also grateful to Dr. Kiyoshi Ueda for valuable comments on decay processes. We would like to thank the staff of the Photon Factory for stable operation of the storage ring. This work was performed under the approval of the Photon Factory Program Advisory Committee (Proposal No. 93G308).

- 
- [1] V. Schmidt, in *X-ray and Atomic Inner-Shell Physics 1982*, Proceedings of the International Conference on X-ray and Atomic Inner-Shell Physics, edited by B. Crasemann, AIP Conf. Proc. No. 94 (AIP, New York, 1982), p. 544.
- [2] T. Hayaishi, E. Murakami, Y. Morioka, E. Shigemasa, A. Yagishita, and F. Koike, *J. Phys. B* **27**, L115 (1994).
- [3] A. Russek and W. Mehlhorn, *J. Phys. B* **19**, 911 (1986).
- [4] G. B. Armen, J. Tulkki, T. Aberg, and B. Crasemann, *Phys. Rev. A* **36**, 5606 (1987).
- [5] F. H. Read and P. Hammond, *J. Phys. B* **21**, 4225 (1988).
- [6] P. van der Straten, R. Morgenstern, and A. Niehaus, *Z. Phys. D* **8**, 35 (1988).
- [7] F. Koike, *Phys. Lett. A* **193**, 173 (1994).
- [8] S. A. Sheinerman, *J. Phys. B* **27**, L571 (1994).
- [9] A. G. Kochur, A. I. Dudenko, V. L. Sukhorukov, and I. D. Petrov, *J. Phys. B* **27**, 1709 (1994).
- [10] T. A. Carlson, W. E. Hunt, and M. O. Krause, *Phys. Rev.* **151**, 41 (1966).
- [11] T. Tonuma, A. Yagishita, H. Shibata, T. Koizumi, T. Matsuo, K. Shima, T. Mukoyama, and H. Tawara, *J. Phys. B* **20**, L31 (1987).
- [12] H. Maezawa, Y. Suzuki, H. Kitamura, and T. Sasaki, *Appl. Opt.* **25**, 3260 (1986).
- [13] Y. Kitajima, Y. Takata, A. Toyoshima, and H. Maezawa, *Rev. Sci. Instrum.* **63**, 886 (1992).
- [14] Y. Morioka, A. Akahori, T. Hayaishi, T. Namioka, T. Sasaki, and M. Nakamura, *J. Phys. B* **19**, 1075 (1986).
- [15] K. Siegbahn, C. Nordling, G. Johansson, J. Hedman, P. F. Heden, K. Hamrin, U. Gelius, T. Bermbark, L. O. Werme, R. Manne, and Y. Bear, *ESCA Applied to Free Molecules* (North-Holland, Amsterdam, 1971), p. 47.
- [16] C. Dezarnaud, F. Guillot, and M. Tronc, *J. Phys. B* **25**, L123 (1992).
- [17] M. Breinig, M. H. Chen, G. E. Ice, F. Parente, B. Crasemann, and G. S. Brown, *Phys. Rev. A* **22**, 520 (1980).
- [18] N. Saito and I. H. Suzuki, *J. Phys. B* **25**, 1785 (1992).
- [19] T. Hayaishi, Y. Morioka, T. Akahori, M. Watanabe, A. Yagishita, and M. Nakamura, *Z. Phys. D* **4**, 3061 (1986).
- [20] P. A. Heimann, D. W. Lindle, T. A. Ferrett, S. H. Liu, L. J. Medhurst, M. N. Piancastelli, D. A. Shirley, U. Becker, H. G. Kerckhoff, B. Langer, D. Szostak, and R. Wehlitz, *J. Phys. B* **20**, 5005 (1987).

- [21] F. Heiser, S. B. Whitfield, J. Viefhaus, U. Becker, P. A. Heimann, and D. A. Shirley, *J. Phys. B* **27**, 19 (1994).
- [22] G. S. Brown, M. H. Chen, B. Crasemann, and C. E. Ice, *Phys. Rev. Lett.* **45**, 1937 (1980).
- [23] G. B. Armen, T. Åberg, J. C. Levin, B. Crasemann, M. H. Chen, G. E. Ice, and G. S. Brown, *Phys. Rev. Lett.* **54**, 1142 (1985).
- [24] O. Keski-Rahkonen and M. O. Krause, *At. Data Nucl. Data Tables* **14**, 139 (1974).